Available online at www.sciencedirect.com
ScienceDirect
Earth and Planetary Science Letters 254 (2007) 404–415
EPSL
www.elsevier.com/locate/epsl

Converted waves reveal a thick and layered tectosphere beneath the Kalahari super-craton

Gérard Wittlinger [a,*], Véronique Farra [b]

[a] E. O. S. T., 5 rue René Descartes, 67084 Strasbourg Cedex, France
[b] IPG Paris, Equipe de Sismologie, case 89, 4 place Jussieu 75252 Paris, France

Received 29 June 2006; received in revised form 29 November 2006; accepted 30 November 2006
Available online 8 January 2007
Editor: R.D. van der Hilst

Abstract

Thick and high-velocity roots are generally observed beneath the Archean cratons. Inside these high-velocity keels, velocity contrasts are detected neither by surface nor by body waves tomographies. We present here evidences based on the S-to-P and P-to-S converted waves for the existence of an irregularly stratified and thick keel beneath the Kalahari super-craton. To satisfy surface wave data and S-to-P conversions, the velocity model should have beneath the Moho a ~160 km thick anisotropic structure with vertical slow axis and decreasing anisotropic parameters with depth. Such a structure may stem from the preferred orientation of olivine [100] axis in the horizontal plane under shearing deformation. This structure, together with the ~100 km thick layer underlying it, forms a ~300 km thick continental root beneath the cratons. Inside this root, the P and S velocities should be higher on average respectively by an amount of 6% and 4% than the AK135 velocity model. Beneath ~300–350 km depth, a low velocity zone is clearly detected that may be either the remainder of large magma reservoirs related to cratonic flood basalts or a melted silicate layer created by the transformation, just above the 410-km deep discontinuity, of wadsleyite assembly to olivine assembly.

Keywords: Kalahari craton tectosphere; S and P-receiver functions imaging

1. Introduction

The Kalahari super-craton is formed by the Archean Kaapvaal and Zimbabwe cratons that are separated by the Limpopo Belt and surrounded in the south by the Proterozoic Namaqua–Natal belt and in the west by the Kheiss Belt (Fig. 1). The Kaapvaal craton is one of the oldest continental blocks on Earth and is the outstanding feature of this collage of cratons and terranes named the Kalahari super-craton. The Kaapvaal craton itself is formed by an aggregation of Archean terranes with distinct structural trends assembled and stabilized between −3.1 to −2.6 Ga. Later, at ~−2.06 Ga, the ultra-mafic Bushveld complex intruded the craton and covered an about 60,000 km^2 large area. The Limpopo Belt is an ancient micro continent, which contains probably the oldest (~−3.8 Ga) basement in Africa, it was squeezed between the Kaapvaal and Zimbabwe cratons during their collision (~−2.7 to −2.6 Ga). During the collision, the Limpopo terrane was thrust

* Corresponding author.
E-mail addresses: Gerard.Wittlinger@eost.u-strasbg.fr (G. Wittlinger), farra@ipgp.jussieu.fr (V. Farra).

0012-821X/$ - see front matter © 2007 Elsevier B.V. All rights reserved.
doi:10.1016/j.epsl.2006.11.048

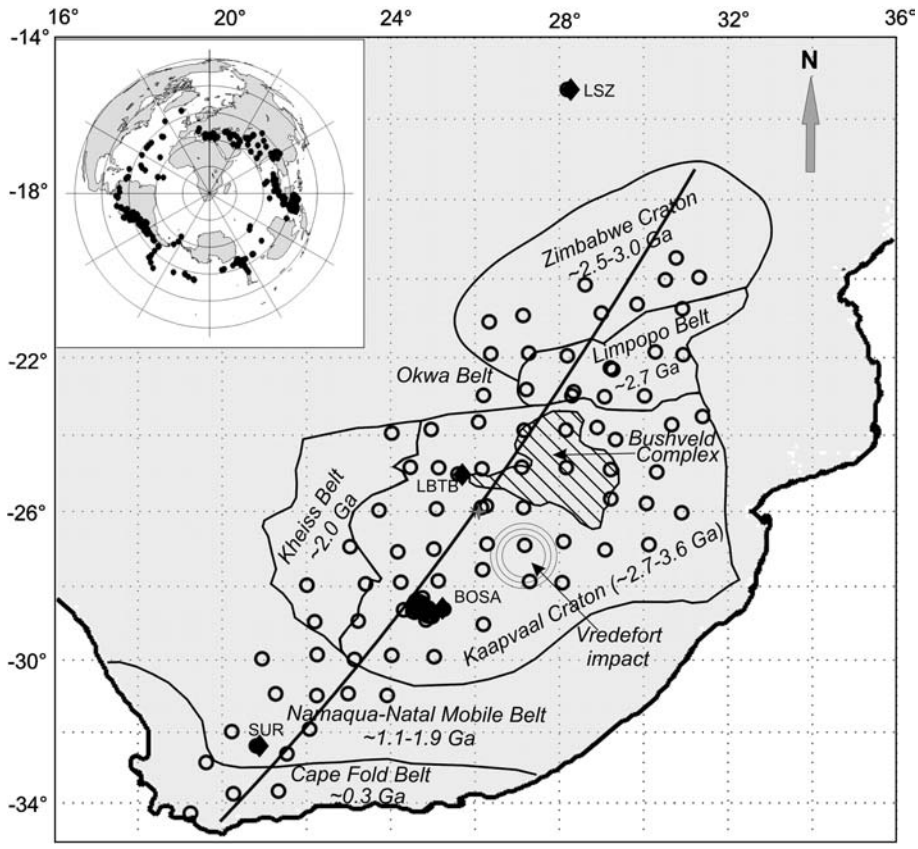

Fig. 1. Situation map with stations location (open circles are mobile stations and diamonds are permanent stations); the cluster near BOSA is the dense Kimberley array. Contours (from [5]) outline cratons and mobile belts. Insert shows the azimuth and distance distribution of the used earthquakes for the S-receiver functions. The black line gives the position of the migration sections, with origin at latitude −26°, longitude +26° (blue star). (For interpretation of the references to colour in this figure legend, the reader is referred to the web version of this article.)

over the Zimbabwe craton and the Kaapvaal craton was thrust under the Limpopo terrane generating a significant crustal thickening [1].

The distinctive seismological characteristic of Archean cratons is their high-velocity keel [2–4]. Beneath the Kalahari super-craton in Southern Africa, high seismic velocities principally obtained from surface and body wave tomographies are reported for the upper mantle. Body wave tomography [5,6] shows a thick and high-velocity root extending down to 300 km depth beneath the Kaapvaal craton and ~200 km beneath most of the Zimbabwe craton. Surface wave tomographies assuming isotropic medium show either a rather uniform high-velocity keel with values up to ~+10% higher than the reference models [7,8], or a high-velocity lid above a lower velocity zone [9–11]. On the contrary, anisotropic surface wave analysis [12,13] shows evidences for the existence of an anisotropic layer with radial symmetry and vertical slow axis that may extend up to 200 km depth. While surface wave tomography has a coarse spatial horizontal resolution, body wave tomography cannot easily detect horizontal or sub-horizontal stratifications due to its inescapable vertical smearing. Nevertheless most of these studies are in keeping with a 200 to 250 km thick uniform high-velocity root beneath the South African cratons. Strikingly there is little or no seismic evidence for the existence of upper-mantle stratifications located between the Moho and the 410-km deep discontinuity. Gao et al. [14] using P-receiver functions seem also to credit this absence of detectable upper-mantle discontinuities. However the P-receiver functions which are blurred by multiples up to ~260 km depth are not appropriate for upper-mantle stratification detection. The velocity gradients located between the Moho and the transition zone are probably weak, their detection therefore remains a challenge. In contrary, the three foremost upper-mantle discontinuities, the Moho, the 410 and the 660-km deep discontinuities, are easily detected with the receiver function technique.

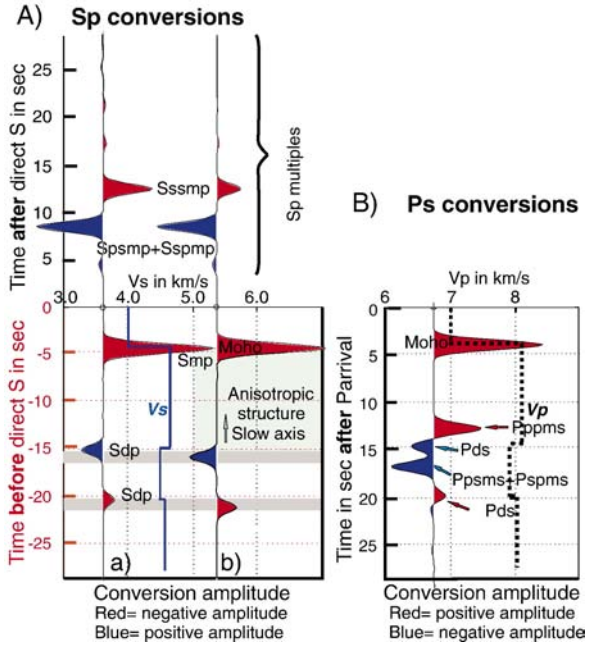

Fig. 2. A) Synthetic S-to-P seismograms (P component) generated in an isotropic (a) and an anisotropic (b) model, calculated with the method of [40]. The sign of the seismograms was reversed in order to make the S-receiver functions similar to the P-receiver functions. The origin of the time axis is at the principal shear-wave arrival. Multiples conversions exist and may be strong, but they arrive after the direct S wave and thus do not interfere with the primary conversions. B) Synthetic P-to-S seismogram (Sv component) in the same isotropic medium as for A) showing that the direct conversions and the multiples arrive all together after the direct P-arrival (time 0). Note the opposite sign of the time axis for the P and S-receiver functions.

Here we shall first attempt to define the thickness of the tectospheric root beneath the Kalahari super-craton. This goal can be achieved with some details due to the reasonably good lateral resolution obtained with the receiver functions migration technique. We also deal with whether the craton keel is a uniform high-velocity feature or whether significant stratifications may be detected. The Bushveld complex, the largest mafic intrusion of the world, is located in the northern part of the Kaapvaal craton. A magma reservoir still present today and located at the base of the tectosphere [15] is probably associated with these huge 2.05 Ga old flood basalts. The receiver function techniques should be able to detect this hypothetical reservoir and to appraise its size. To achieve these goals, we shall use mostly the S-to-P conversions (S-receiver functions), not only because they are free from multiples but also because their amplitude may be higher than the corresponding P-to-S conversions (P-receiver functions). To support the S-receiver functions we use in addition the P-to-S conversions in the time or depth intervals where they are not polluted by the strong Moho multiples.

2. Data and method: mutual assessment of the S and P-receiver functions

Here we present a view of the upper-mantle structure beneath the Kalahari super-craton based mainly on the S-to-P conversions. We use the data collected during the Kaapvaal and Kimberley seismic experiments (http://www.iris.edu/SeismiQuery/ and http://www.dtm.ciw.edu/mantle/kaapvaal/) in addition to the data of four permanent stations (SUR, BOSA, LBTB and LSZ). Using a signal/noise ratio criterion, we selected the events with magnitude Mw higher than 5.7, but mostly higher than 6.0, and with epicentral distances between 55° to 110° for the S-receiver functions and between 40° to 95° for the P-receiver functions. These earthquakes are fairly evenly distributed versus back azimuth and epicentral distance (Fig. 1) and provide about 5000 S-receiver functions (here after named SRFs).

The SRFs [16] are the equivalents for the S-to-P conversions of the nowadays well-known P-receiver functions (here after named PRFs). They are well adapted for imaging seismic velocity contrasts in the upper mantle since all the S-to-P conversions are precursors of the direct shear wave while all the multiples arrive later than the direct S wave (Fig. 2-A). This is a quite different situation than for the PRFs blurred by strong crustal multiples (Figs. 2-B and 3-A). The SRFs are computed using low-frequency filtered data (0.125–0.03 Hz) with a time domain iterative deconvolution [17] of the P component by the shear-wave source-function isolated on the Sv component. The precise identification of the selected shear-wave source, namely S or SKS phases, is important since their ray parameters differ strongly from one another. Around the epicentral distance of 83°, the S and SKS phases overlap and the ScS phase arrives significantly later with smaller amplitude. The contamination of the S-to-P conversions by other seismic phases is discussed in [18]. In the distance range of 81° to 85°, we inspected visually each seismogram to decide which of the S or SKS phases should be used for the deconvolution. Most of the SRFs in the narrow distance range of 82° to 84° were discarded. In the migration process we use the ray parameter corresponding to the phase (S or SKS) used for the deconvolution. If the time and the amplitude axes are reversed for the SRFs, they look like the PRFs (except in the time interval of the crust multiples, see Fig. 2). In isotropic media, the P-to-S and the S-to-P transmitted waves are only sensitive to the shear-wave

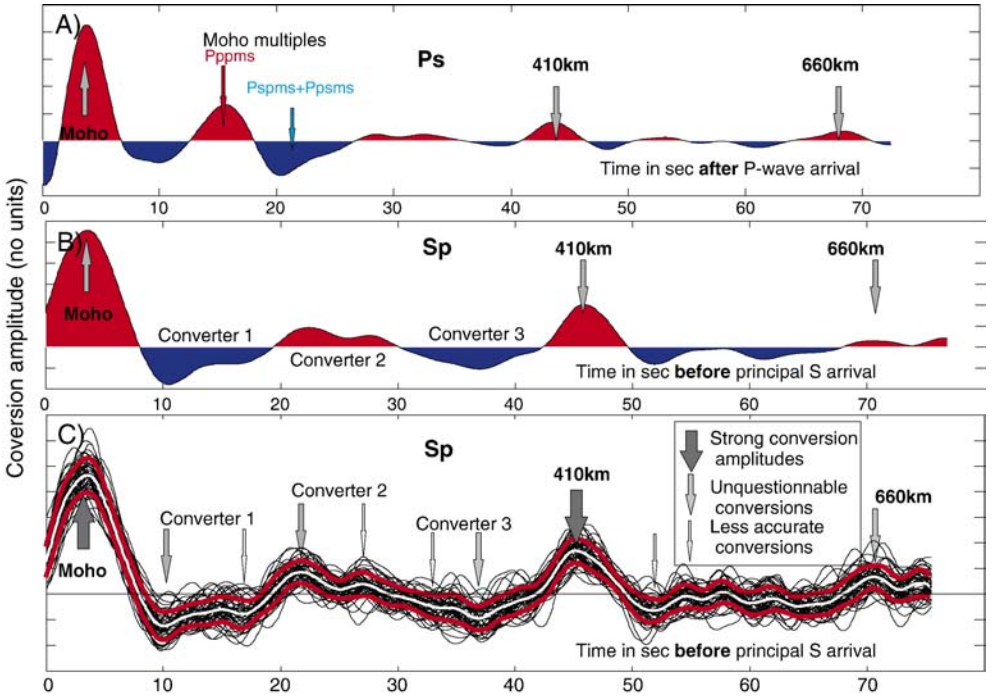

Fig. 3. Move-out corrected stacks of the PRFs (Sv components) (A) and the SRFs (P components) (B) for the stations located on the Kaapvaal craton. Time 0 corresponds to the principal P (PRFs) and S (SRFs) arrivals. A reference ray parameter of 7.5 s/° is used. The epicentral distances are larger than 80° for the SRFs and 55° for the PRFs in order to recover the conversions for interfaces as deep as the 660-km discontinuity. For the SRFs stack, the time and the amplitude axes are reversed so that, for both kinds of RFs, the red (respectively blue) color stands for positive, (respectively negative) downward velocity gradients (as in Fig. 2). The red (respectively blue) arrows in Fig. A give the theoretical arrival times of the two main Moho multiples (Pppms, Ppsms+Pspms) for a Moho at a mean depth of 35 km. (C) "Bootstrap" move-out corrected stacks for the same dataset as in (B), white line is the mean stack and red lines correspond to ± one standard deviation from the mean (90% confidence level).

velocity contrasts and gradients. A downward positive (respectively negative) velocity contrast produces positive (respectively negative) converted-wave amplitude on the two kinds of receiver functions.

To enhance the conversions having some spatial continuity and to reduce the noise probably spatially incoherent, we use two stacking techniques, one in the time domain and the other in the depth domain. First, we perform a move-out corrected stack of a bundle of RFs (Figs. 3 and 4) to obtain an average RF over the retained back azimuths and distances. The S-to-P converted waves have great emerging angles so that the conversions occur far from the station, at about a horizontal distance equivalent to the depth of the conversion point. For this reason, the stacks (Figs. 3-B and 4-a,b,c) are smoothed means relevant for hundreds of kilometers of lateral extend all around the stations. This is particularly valuable for the stacks (Figs. 3-B and 4-b and c) involving numerous stations themselves spread-out over great distances.

We appraise the ability of the SRFs to detect weak converters using a bootstrap-like method. In order not to introduce large dissimilarity in the RFs due principally to strong differences in the tectonic setting, the stations used for this evaluation are restricted to the Kaapvaal craton. The bootstrap stacks combine the contribution of the strictly spoken "seismic noise" that is present in each individual RF with the variability of the RFs due to the lateral variability of the converters. We use only great epicentral distances ($\Delta > 80°$) in order to include conversions from the transition zone. A primary set of ~2500 SRFs is used and divided into ~50 subsets, each one composed of ~125 RFs randomly selected among the primary set. A move-out corrected stack is then performed on each data subset and the result plotted, allowing the determination of the mean and of the standard deviation (Fig. 3-C). The Moho, the 410-km deep discontinuity and three converters located between the Moho and the "410" are significantly detected with a confidence level of ~90% corresponding to the mean plus or minus one standard deviation. Other conversions are less accurately detected as for example the 660-km deep discontinuity and structures in the transition zone.

We also perform a three-dimensional common conversion point (CCP) migration [17] using a modified (see

below) AK135 velocity model [19]. The output of this CCP migration is a 3-D image of the upper mantle beneath the array of stations in which each elementary cell is assigned with the averaged amplitude of all the conversions that occurred in this cell. Finally, the vertical sections, oriented N30°E, are obtained by averaging horizontally and perpendicularly to the section the conversion amplitudes that occurred beneath the selected tectonic units (Figs. 5, 6, 7, 8, 9 and 10). This is why these sections bear the inescapable drawback of representing laterally tilted or buckled interfaces as thickened interfaces. We use a blue–white–red color code to represent the conversion amplitudes, with blue (respectively red) color corresponding to downward negative (respectively positive) impedance contrasts in either PRFs or SRFs migrations, providing the amplitude sign has been reversed on the latter.

Remain to determine the smallest size of the imaged converters that can be interpreted. The first Fresnel zone of the converted waves gives a good estimate of this lower scale i.e. of the horizontal resolution. On the other hand, the vertical resolution is determined by the wavelength and not by the Fresnel zone because the vertical position of the converters follows from the travel-times. The Fresnel zone has an elliptic section whose half axes' lengths are given by $r_{\mathrm{par}} = \sqrt{\frac{\lambda z}{\cos^3 i_R}}$ and $r_{\mathrm{nor}} = \sqrt{\frac{\lambda z}{\cos i_R}}$ respectively for the axis in the plane of incidence and for the axis perpendicular to this plane [20], where λ stands for the wavelength of the converted wave (S wave for P-to-S conversions and P wave for S-to-P conversions), z for the depth of the converters and i_R for the emerging angle of the converted wave. As the back azimuths of the used earthquakes are varying (see insert in Fig. 1) we shall approximate the Fresnel zone by a circular horizontal section with a radius equal to $(r_{\mathrm{par}}+r_{\mathrm{nor}})/2$. The size of this Fresnel zone increases with depth and is ~4 times greater for the S-to-P conversions than for the P-to-S conversions. Short epicentral distances, i.e. great incidence angles, may lead to very large Fresnel zones especially for the S-to-P conversions. The radius of the approximately circular Sp Fresnel zone, computed for example for an epicentral distance of 80°, a focal depth of 33 km and for 100, 200, 300 and 400-km deep converters are respectively 105, 160, 290 and 380 km. These values give the minimum lateral size of the converters that can be interpreted for each depth range.

Owing to these remarks, migration should best be performed using cells with size increasing with depth. However, we use an alternative option by performing the migration with constant-size cells then by smoothing laterally the depth-sections. In Figs. 7 and 8 the smoothing-kernel we use extends over lateral distance

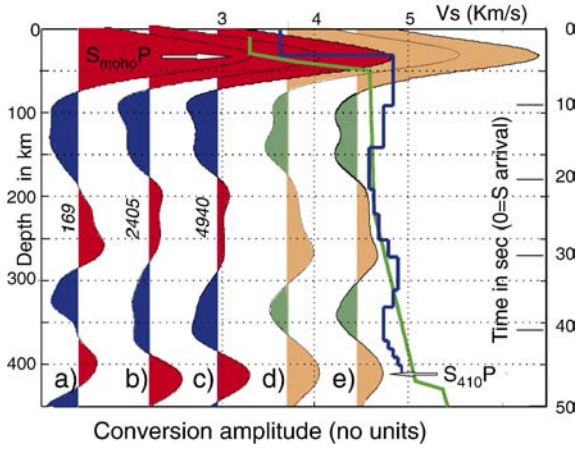

Fig. 4. Move-out corrected stack of the SRFs (P component) (a) at station BOSA, (b) at all stations located on Kaapvaal craton (including stations of Kimberley array) and (c) at all stations of Kaapvaal network (107 stations), including stations SUR, BOSA, LBTB and LSZ. A reference slowness 8.4 s/° is used. Number in *italic* beside the stack indicates the number of RFs involved. (d) Synthetic SRF computed using the isotropic velocity model indicated in blue. (e) Synthetic SRF computed with an anisotropic model (Fig. 8-B) similar to the model in [13], deeper than 200 km this model is the same as for (d). The reference model AK135 is indicated in green. Conversion of the time scale (on right side) to the depth scale (on left side) is done using the AK135 model.

that corresponds to the mean radius of the Fresnel zone at a given depth. The PRFs migration has a much better lateral resolution than the SRFs migration, but fails strongly in imaging the upper mantle due not only to the presence of strong multiples but also to their higher frequency content, inadequate to detect gradual boundaries. Moreover, the strong anelastic attenuation of the S waves pleads also for stronger SRFs than PRFs.

3. Results: a thick and layered craton keel

If the SRFs and the PRFs migrations are both performed with a velocity model close to the effective one, then the converters are imaged at the same depths with both migrations. Conversely, the true mean velocity model can be retrieved by perturbing the velocity model until some selected and well-imaged converter coincides in both migrations. The outstanding and clear 410-km deep discontinuity is well suited for this velocity-model adjustment. For the 410-km deep discontinuity, the PRFs migration with the standard AK135 model gives a mean depth of ~400 km. A significant deeper mean depth of ~425 km is obtained with the SRFs migration (Fig. 5-A and B). Due to the dissimilarity of the emerging angles of the respective

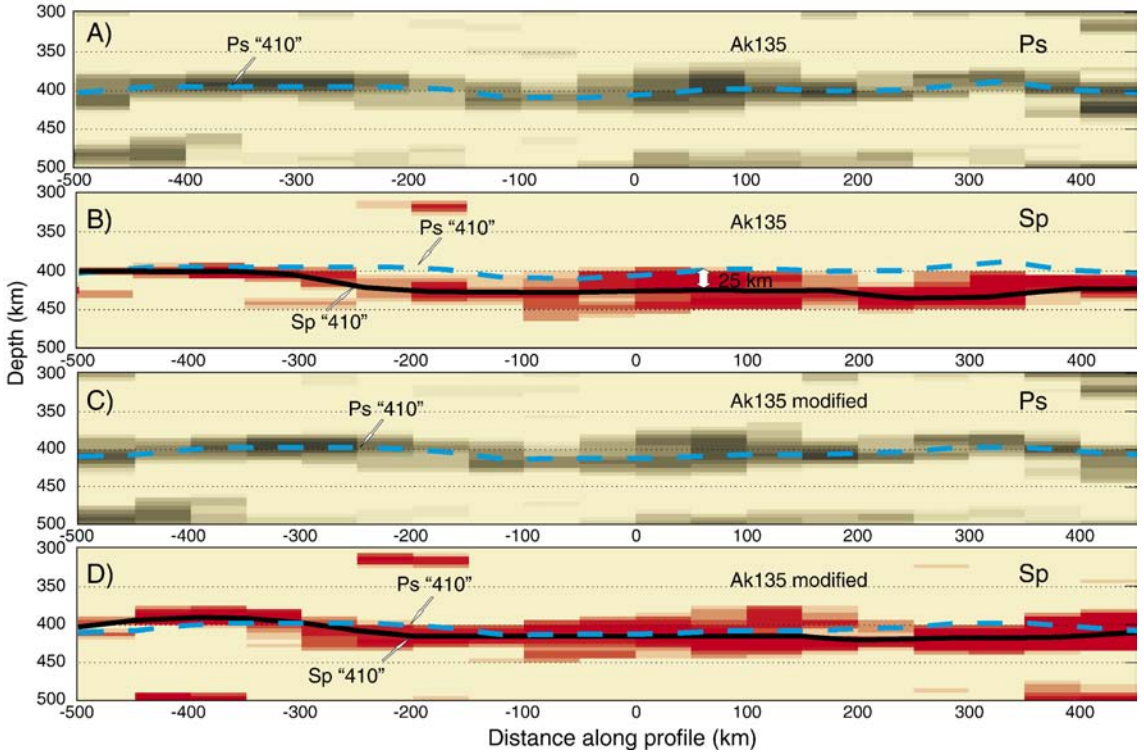

Fig. 5. Common conversion point (CCP) migration of low-frequency P and S-receiver functions restricted to the Kaapvaal craton and to a depth interval around the 410-km deep discontinuity. For the save of clarity only the positive conversions are displayed, in black for the Ps and in red for the Sp. Both migrations are performed with the standard AK135 velocity model (sub-Fig. A and B) and with a modified AK135 model (sub-Fig. C and D) in which P-velocity is 6% and S-velocity is 4% higher than the velocities of the standard model. Black heavy and blue dotted lines underline the 410-km deep discontinuity determined respectively with SRFs and PRFs migrations.

converted rays, the effect of a change in the velocity model is different on either PRFs or SRFs migration. For the PRFs migration the converters are mainly moved up or down while for the SRFs migration the converters are moved more laterally and only slightly up or down. Owing to this, the depth discrepancy of the 410-km deep discontinuity may be corrected (using a grid-search method) by increasing in the AK135 velocity model the P-wave velocity by ~6% and the S-wave velocity by 4% (Fig. 5-C and D) leading to a S-wave velocity (~4.65 km/s) at 200-km depth consistent with the velocity inferred from mantle–xenoliths [21]. We conclude that beneath the South African super-craton the upper-mantle velocities seem to be on average significantly higher than the velocities of the AK135 model in agreement with the tomographic results [5,11]. Beneath the Moho, the modified AK135 velocity model in keeping with the previous observations is used for the migrations and the move-out stacks.

In order to define clearly the depth interval where the Moho multiples (Ppp_ms and Psp_ms+Pps_ms) preclude any imaging of converters, we image the medium up to 60-km depth using the CCP migration of high frequency PRFs (Fig. 6-A and B). We use a mean P-wave velocity of 6.5 km/s in the crust [22] and a constant Vp/Vs ratio of 1.75. The Moho appears as a thin, less than ~5 km thick and well-defined interface. The mean thickness of the crust is ~35 km beneath the cratons (Fig. 6-B); the crust is thickened up to 45 km beneath a broad zone encompassing the Bushveld complex, but much larger than its surface manifestation, and beneath the southern part of the Zimbabwe craton. Under the Bushveld complex, weak conversions are associated with the thickening of the crust and are probably due to the high-velocity underplated mafic granulites [23] that reduce the velocity contrast between the lower-crust and the upper mantle. The Limpopo Moho is slightly shallower than the Moho beneath the two adjacent cratons. This supports the inference that the Limpopo terrane was overthrusted on the Zimbabwe craton and that the Kaapvaal craton was underthrusted beneath the Limpopo terrane. Beneath the younger belts, the Moho is significantly deeper (Fig. 6-A). This is obvious beneath the subduction related Namaqua

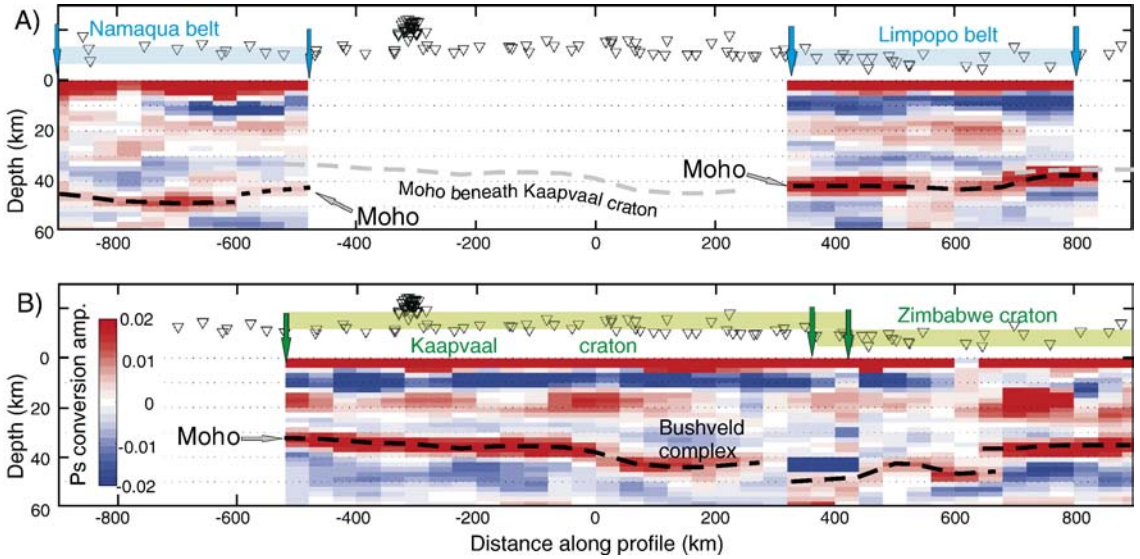

Fig. 6. CCP migration of high frequency (2 to 0.1 Hz) PRFs (radial component) projected along a profile oriented N30°E and centered at lat=−26° and lon=+26° (black line and blue star in Fig. 1) with vertical exaggeration of a factor 5. A) Only the conversions occurring strictly beneath the Namaqua Mobile Belt and the Limpopo Belt are stacked in this section. B) Same as A) for the Kaapvaal and Zimbabwe cratons. We do not consider the conversions occurring at the edges of the area, i.e. the Cape fold belt, the Kheiss Belt and the most northern part of the Zimbabwe craton, where ray crossing is too scanty. The limits of the structural units are the same as in Fig. 1. Vertical green and blue arrows indicate the approximate limits of respectively the cratons and the mobile belts. Only cells (size: 50 km in horizontal direction, 2 km in vertical direction) with more than 10 ray hits are considered. Red (respectively blue) colour stands for positive (respectively negative) velocity contrast. Triangles are the projection of the stations on the profile.

Mobile Belt where the Moho reaches a depth of ~48 km, leading to a huge ~10-km step separating the Namaqua and Kaapvaal Moho. The Moho Ps-multiples (Fig. 7) clearly mimic this step and are also weakened beneath the Bushveld complex. Our results concerning the crustal thickness and the amplitudes of the P-to-S conversions at the Moho are in good agreement with earlier studies [24,25]. The slight discrepancy observed at some places between the Moho depth obtained in this study and the one obtained by [25] follows probably from the spatial variations of the Vp/Vs ratio. These variations, from 1.66 to 1.82 [25], are not taken into account in our migration. A high Vp/Vs ratio in the crust rises up the Moho in the migration image while a low ratio deepens it. Taking into account the variations of Vp/Vs would have the effect of smoothing the Moho depth variations since Vp/Vs seems to be high beneath the Bushveld complex (where we obtain a thick crust) and low mostly in the southern part of the Kaapvaal craton (where we obtain a thin crust). However, the Kaapvaal experiment is not really designed for a precise Moho-imaging with CCP-migration techniques: the station's spacing (80 to 100 km) is too large for the multi-fold coverage with converted waves to be achieved in the crust.

The Ps Moho multiples beneath the Kalahari supercraton have unusually strong amplitudes stemming principally from the sharpness of the Moho interface. They dominate completely the PRFs-migrated section in the depth interval of ~90 to ~220 km beneath the Kaapvaal and Zimbabwe cratons and the Limpopo Belt and in the depth interval of ~150 to ~260 km beneath the Namaqua Belt. Except for these depth intervals, both migrated sections performed either with the PRFs or the SRFs (Figs. 7 and 8 respectively) show very similar structures although some noticeable but local differences in amplitude strength are present. Because the Pps_ms+Psp_ms Moho multiples (with negative amplitude) erase the upper part of the positive converter located in the depth range of ~180 to ~260 km, we only detect the lower part of this converter on the Ps-section. A similar observation stands for the negative converter located just beneath the Moho, which appears thinner on the Ps-section than on the Sp-section. The exceptionally strong positive amplitude Ppp_ms Moho-multiple erases completely the base of this negative converter except beneath the Namaqua Belt (between km −500 and km −900 in Fig. 7-A) where the Moho is deeper and therefore also the depth interval polluted by the multiples.

Owing to the comparison between Ps and Sp synthetics (Fig. 2), between the two move-out corrected stacks (Fig. 3) and between the PRFs and the SRFs

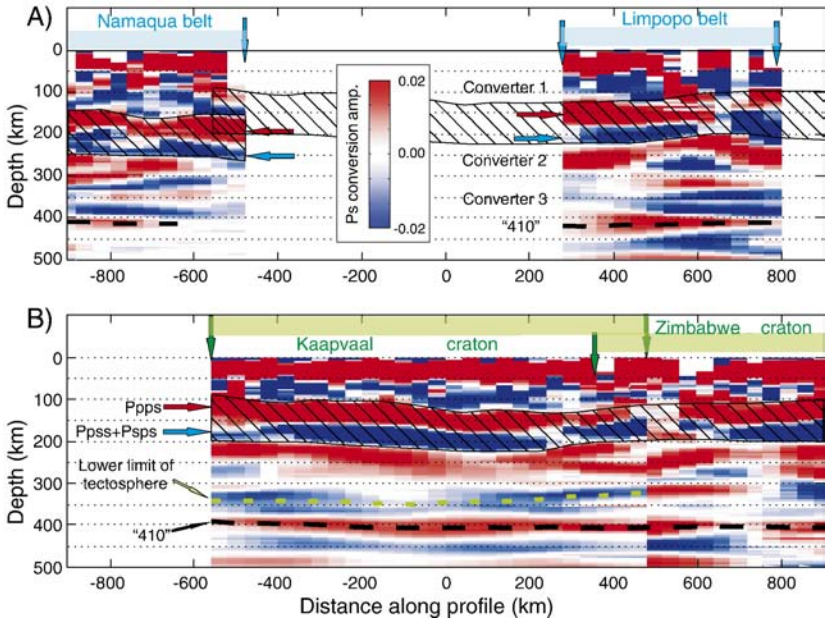

Fig. 7. Same as Fig. 6 but relative to low frequency (0.125 to 0.03 Hz) PRFs (here Sv component). The red and blue arrows in sub-figures A and B indicate the position of the Moho multiples and the hatched polygons the area where the Moho multiples conceal the converters. The 410-km deep discontinuity and the inferred base of the tectosphere are underlined with respectively black and green dotted lines. Cell sizes are of 40 km in horizontal direction and 10 km in vertical direction.

migrations, our confidence in the imaging with receiver functions is strengthened. Moreover, the CCP migrations help to better appraise the spatial continuity and the size of the conversion levels.

Between the Moho and the 410-km deep discontinuity the SRFs move-out corrected stacks (Figs. 3-B and 4-a,b, c) show three arrivals that seem to be enlarged or split into two pulses. Moreover the mean conversion amplitude at

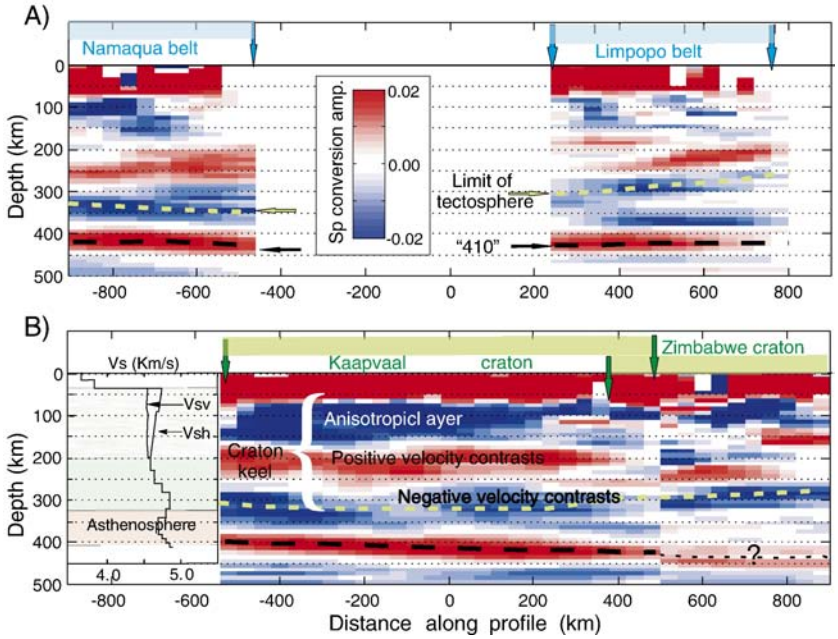

Fig. 8. Same as Fig. 6 but relative to low-frequency (0.1 to 0.03 Hz) SRFs (P component). The shear-wave radially anisotropic velocity model is displayed on the left side of B.

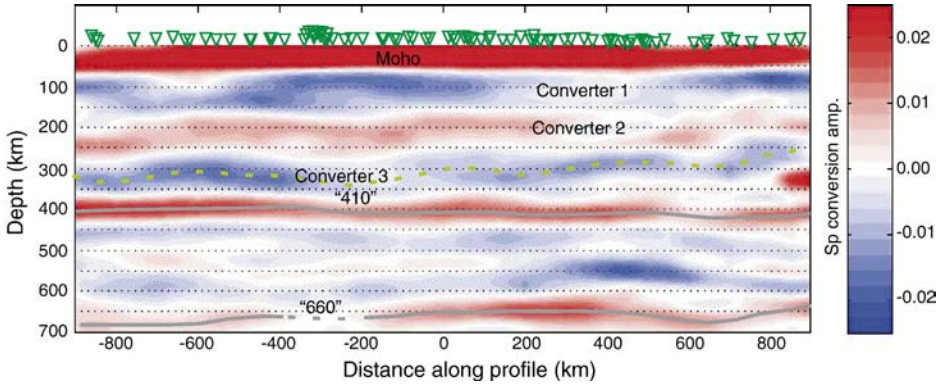

Fig. 9. Smoothed (~200 km in horizontal and ~40 km in vertical directions) CCP migration of low-frequency (0.1 to 0.03 Hz) SRFs (P component, epicentral distances >80°, conversions of S and SKS phases are used). This section is relative to the whole South Africa super-craton including the cratons and the mobile belts. Grey lines underline the 410 and 660-km deep discontinuities, green dotted line stands for the inferred base of the tectosphere.

the two deeper levels changes if the number of stations involved in the stack increases (Fig. 4-b, and c) reflecting the fragmentation and/or unevenness over great distances of the converting levels. The CCP migration (Figs. 7 and 8) enhances the spatial variability of the converters. The fragments of the three main conversion levels are located at a depth ranging from 80 to 160 km for the upper negative level (converter 1), from 180 to 260 km for the positive intermediate deep level (converter 2) and from 300 to 360 km for the negative deepest level (converter 3) (Fig. 9). Strikingly, Fig. 8 shows that on average the Limpopo Belt and even the Namaqua Belt upper-mantle structures bear a similarity with the Kaapvaal craton structure. On the contrary, the Zimbabwe craton seems to have a quite different upper-mantle structure even if the three main converting levels are present. Similar observation stands also for the PRFs-migrated sections (Fig. 7) especially for structures in the vicinity of the 410-km deep discontinuity.

The conversion amplitude is roughly proportional to the S-wave impedance contrast (assuming isotropic medium) and depends also on the incidence angle. The impedance contrast at a conversion level may be estimated relatively to a reference impedance contrast if the incidence angles at the two levels are not too different. Information on the S-velocity contrast ($\delta Vs = \sim +0.81$ km/s) at the Moho is available [26]. Synthetic modeling using this velocity contrast gives the same conversion amplitude

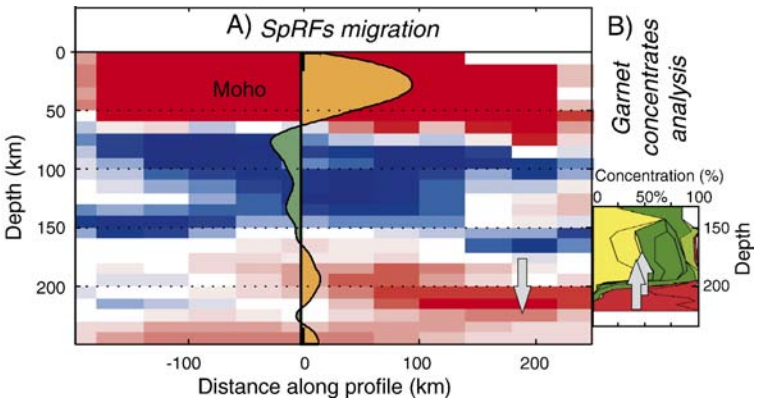

Fig. 10. A) CCP migration of SRFs (centered at 27°S, 27°E and projected along a profile oriented N30°E) restricted to the conversions occurring in the vicinity of the Vredefort impact zone. A move-out corrected stack restricted to some stations located near the center of the area is superimposed. B) Garnet concentrates analysis (after [1]) from kimberlites (Kroonstadt samples, collected near the center of the impact zone) giving the composition with respectively yellow, green and red colors representing the percentage of depleted, fertile and melt-metasomatised rocks. Grey arrow in both subplots indicates the direction of the positive velocity gradient deduced either from SRFs or from kimberlite analysis.

at the Moho as the observed (see Fig. 4d). Using the conversion amplitude at the Moho as reference, the estimated S-velocity contrasts deduced from the move-out corrected stack at all stations located on the Kaapvaal craton (Fig. 3-B or C) are respectively ~−0.21 km/s between 80 and 160-km depths, ~+0.14 km/s between 180 and 260-km depths and ~−0.16 km/s between 300 and 360-km depths. A downward negative velocity contrast at ~350-km depth was observed with the S-to-P conversions [27] and was attributed to a local low velocity body (δVs=−0.4 km/s) located NE of the station BOSA and related to flood basalts. Our large scale study shows that this low velocity layer exists beneath most of the Kalahari super-craton, but corresponds on average to a significantly smaller than −0.4-km/s velocity contrast. Synthetic modeling using an isotropic velocity model in keeping with the above observations produces synthetic SRFs (Fig. 4-d) in fairly good agreement with the observations (Fig. 4-a).

The lithospheric keel of the cratons may be defined as the cold, highly depleted and therefore with fast seismic velocities, upper mantle. The seismic tomography, probably due to its too poor vertical resolution, failed until now in determining unambiguously the keel thickness; no low velocity asthenospheric layer – evidence for the base of the keel – could be found with this technique. In contrary, the RFs exhibit beneath the Kalahari super-craton a conversion with negative amplitude, namely the converter 3 that could be interpreted as the bottom of the keel, itself formed by the stack of the two layers imaged with the RFs as the converters 1 and 2. Therefore the South African craton keel may be on average ~300-km thick.

4. Discussion and conclusion

The forsterite content of olivine (%Fo) in the lithospheric mantle beneath South Africa cratons has been determined by inverting olivine–garnet thermobarometer [1,28–30] and consequently the distribution with depth of the depleted, the fertile or the metasomatised rocks. The shear-wave velocity depends on the composition of the rocks. Generally the seismic velocities are faster in depleted rocks than in fertile rocks, which in turn have faster velocities than basaltic melted and metasomatised rocks [29]. As the percentage of these different types of rocks varies with depth, the variation of the composition may explain by itself some of the S-to-P conversions. Moreover steep and significant gradients appear in the distribution of olivine composition with depth [1] implying necessarily concomitant velocity contrasts. The olivine–garnet thermobarometer provides a kind of chemical well-logging relevant for the past (before the last kimberlite eruption at ~100 Ma) upper-mantle composition while the RFs provide a seismic image of the present-day velocity contrasts. The Kalahari super-craton had a lengthy and complex history with a succession of huge tectonic events that may have changed its structure. But the fairly good agreement between the past compositional structure and the present-day structure as imaged with body waves tomography [5] for example may indicate that at least up to a depth of ~200 km there was no or only undetectable evolution of the sub-cratonic structure since the last kimberlite eruption. The Vs-depth profile deduced from cratonic xenoliths (Fig. 10 in [29] for example) is quite similar to the Vsh-depth profile shown in Fig. 8-B down to ~200 km.

However, at some places the velocity profiles deduced from the composition and from the RFs are in strong disagreement. For example, the thermobarometric data [1] from samples collected near Kroonstadt (in Vredefort impact region) show at ~200-km depth a steep gradient in the composition percents, from depleted (higher velocity) to metasomatised (lower velocity) minerals implying a steep downward negative gradient in shear velocity. At that depth, the SRFs show rather positive conversion amplitudes (Fig. 10), evidences for positive velocity contrasts. The apparent high temperature and fertile composition is probably due to metasomatism processes occurring at the time of the eruption [30]. The high-T and fertile composition may thus be only localized around the kimberlite pipes and is not a regional phenomenon detectable with the SRFs. A similar puzzling situation was already observed beneath the Baltic Shield [31].

The surface wave tomographies assuming isotropy [8–10] do not image the velocity contrasts displayed by the SRFs for depths between 80 and 200 km. The question remains why; are the velocity contrasts too weak? Another cause producing S-to-P conversions could be found to account for this discrepancy. Anisotropy contrasts, not detected or misinterpreted by isotropic surface wave analysis, generate wave conversions. A layer with radial anisotropy, either with vertical slow (Vsv<Vsh) or fast (Vsv>Vsh) axis, embedded in isotropic layers, generates S-to-P conversions. If the vertical axis is slow, the converted amplitude is negative or positive respectively at the incoming or outgoing interface. Such a radial anisotropic layer with a slow vertical axis and located in the upper mantle beneath the Moho was detected with anisotropic surface wave analysis [12,13]. Forward modeling using a model that incorporates such anisotropy in the mantle, [(Vph−Vpv)/Vpv~+7%, (Vsh−Vsv)/Vsv~+3%] below the Moho, these anisotropic quantities decreasing with depth down to 200 km (sketched on the

right side of Fig. 8-B), produces synthetic SRFs (Fig. 4-e) in a reasonably good agreement with the observations. Such an anisotropic model satisfies both the SRFs and the surface wave data [13]. At least two main physical processes may be responsible of the observed radial anisotropy, namely a small-scale periodic layering or the preferential orientation of minerals that are by themselves anisotropic like olivine. In both cases, the vertical direction is slow, and the horizontal directions are fast on average. These two kinds of models are yet different by the variations, with respect to the source azimuth, of the conversion amplitudes they may generate. We observe on the SRFs some amplitude variations of the conversions with respect to the source azimuth, but in order to discriminate which of the two models fit the data better, a proper separation, not done here, of the Sh-to-P and the Sv-to-P conversions is required (see [16]). In any case, a model with preferential orientation of the minerals, having anisotropy parameters similar to those we obtain with the forward modeling [(Vsh − Vsv)/Vsv ∼ +3% under the Moho, this anisotropic parameter decreasing with depth until 200-km depth] would give SKS-splitting parameters in agreement with the observations reported in [32].

Recent models [15] of cratonic flood basalts imply the presence still today of melt zones located at the base of the tectosphere that may correspond to the negative gradient zone we detect at about 350-km depth. The 350-km deep negative converter (converter 3) may be interpreted as the image of the top of a giant basaltic reservoir that has formerly fed the flood basalts [21,33]. But this negative converter seems to extend beneath the whole super-craton and thus its interpretation as the top of a unique reservoir may be inappropriate. An alternative interpretation could be found in the transformation, just above the 410-km deep discontinuity, of wadsleyite assembly into olivine assembly accompanied by water release [34]. This transformation may create a thin low velocity layer, relatively stable in time, of (partial) molten silicate [35] whose ceiling is detected with the receiver functions as a negative gradient. Global seismic tomography [36,37] would probably not be able to image such a thin – some tens of kilometres [34] – layer in contrary to the RFs that are sensitive to the steep velocity gradients. Moreover, the lateral extend of the converter 3, which is over hundreds of kilometres, pleads also for its interpretation as a melted silicate layer overlying the transition zone.

How thick is the lithosphere beneath the South African super-craton? The negative impedance contrast (converter 3) observed at ∼350-km depth implies a ∼300-km thick lithosphere on average. While beneath the cratons and the oldest belts (∼2.0 to ∼3.6 Ga) a ∼300-km thick lithosphere is in keeping with previous results, such a thickness is not expected beneath younger mobile belts. The green dotted line (Fig. 8) shows that the ∼300-km thick lithosphere, we may call tectosphere owing to its thickness, is gently thinning northward beneath the Limpopo Belt (∼2.7 Ga) but less southward beneath the much younger Namaqua–Natal belt (∼1.1 to ∼1.9 Ga). However, as the migration process of the receiver functions smoothes the interfaces over a horizontal scale corresponding approximately to the first Fresnel zone (here ∼300 km for the Sp), the lithosphere–asthenosphere boundary is laterally smoothed. Moreover, since the Mobile Belts are located at the borders of the studied area, our imaging technique is not able, because of the poor ray crossing at the edges, to detect the possible thinning of the tectosphere. Jordan [2] estimated the thickness of the tectosphere at ∼400 km. More recent estimations based on geochemistry [38] and heat flow data [39] give a thickness of ∼250 km. Our estimation, based on the determination of the mean upper-mantle velocities and RFs imaging gives ∼300 km. The thick root, observed beneath the Kalahari super-craton, seems to be not disrupted by convection and is probably stabilized by the depletion of the upper mantle, thus leading to the high velocities we observe. This observation is in keeping with Jordan's tectosphere hypothesis.

In summary, the simultaneous use of S and P-receiver functions shows that the tectosphere beneath the South African super-craton is about 300-km thick on average and stratified. The upper part of the craton keel is a ∼160 km thick anisotropic structure and the lower part a ∼100-km thick positive velocity gradient layer. The Kalahari super-craton tectosphere has significantly (up to ∼+6% for P wave) higher velocities than the reference model AK135. This stratification seems to be the clearest beneath the Kaapvaal craton. Moreover, beneath the keel, we image a negative velocity gradient at about 350-km depth that could be interpreted alternatively as the top of the remainders of the giant basaltic reservoir that formerly fed the flood basalts or as the ceiling of a layer of dense molten silicates generated by the transformation at the 410-km deep discontinuity of wadsleyite assembly into olivine assembly.

Acknowledgments

We thank Matt Fouch for his thoughtful review that helps us to improve significantly the manuscript and we thank also an anonymous reviewer. Many people (http://www.dtm.ciw.edu/mantle/kaapvaal/) were associated in the South Africa seismic experiment, we thank them all for giving the free access to the interesting and high quality acquired data.

References

[1] W.L. Griffing, S.Y. O'Reilly, L.M. Natapov, C.G. Ryan, The evolution of the lithospheric mantle beneath the Kalahari Craton and its margins, Lithos 71 (2003) 215–241.

[2] T.H. Jordan, The continental tectosphere, Rev. Geophys. Space Phys. 13 (1975) 1–12.

[3] T.H. Jordan, Structure and formation of the continental tectosphere, in: M.A. Menzies, K.G.K. Cox (Eds.), J. Petrology, Special Lithosphere Issue, Trans. R. Soc. London, London, United Kingdom, 1988, pp. 11–37.

[4] A.L. Lerner-Lam, T.H. Jordan, How thick are the continents? J. Geophys. Res. 92–13 (1987) 14007–14026.

[5] D.E. James, M.J. Fouch, J.C. Van Decar, S. van der Lee, Kaapvaal Seismic Group, Tectopheric structure beneath Southern Africa, Geophys. Res. Lett. 28–2 (2001) 485–488.

[6] M.J. Fouch, D.E. James, J.C. Van Decar, Mantle seismic structure beneath the Kaapvaal and Zimbabwe cratons, S. Afr. J. Geol. 107–1–2 (2004) 33–44, doi:10.2113/107.1–2.33.

[7] J. Ritsema, H. van Heijst, New seismic model of the upper mantle beneath Africa, Geology 28–1 (2000) 63–66.

[8] K. Priestley, D. McKenzie, E. Debayle, The state of the upper mantle beneath southern Africa, Tectophysics 416 (1–4) (2006) 101–112.

[9] X. Qiu, K. Priestley, D. McKenzie, Average lithospheric structure of South Africa, Geophys. J. Int. 127 (1996) 563–587.

[10] K. Priestley, Velocity structure of the continental upper mantle: evidence from Southern Africa, Lithos 48 (1999) 45–56.

[11] A.M. Larson, J.A. Snoke, D.E. James, S-wave velocity structure, mantle xenoliths and the upper mantle beneath the Kaapvaal craton, Geophys. J. Int. 167 (1) (2006) 171–186.

[12] M. Freybourger, J.B. Gaherty, T.H. Jordan, Structure of the Kaapvaal craton from surface waves, Geophys. Res. Lett. 28–2 (2001) 489–492.

[13] R. Saltzer, Upper mantle structure of the Kaapvaal craton from surface wave analysis—a second look, Geophys. Res. Lett. 29–6 (1093) (2002), doi:10.1029/2001GL013702.

[14] S.S. Gao, P.G. Silver, H.L. Liu, Kaapvaal Seismic Group, Mantle discontinuities beneath Southern Africa, Geophys. Res. Lett. 29–10 (1491) (2002), doi:10.1029/2001GL013834.

[15] P.G. Silver, M.D. Behn, K. Kelley, M. Schmitz, B. Savage, Understanding cratonic flood basalts, Earth Planet. Sci. Lett. 245 (1–2) (2006) 190–201.

[16] V. Farra, L. Vinnik, Upper mantle stratification by P and S receiver functions, Geophys. J. Int. 141 (2000) 699–712.

[17] G. Wittlinger, V. Farra, J. Vergne, Lithospheric and upper mantle stratifications beneath Tibet: new insights from Sp conversions, Geophys. Res. Lett. 31 (L19615) (2004), doi:10.1029/2004GL020955.

[18] D.C. Wilson, D.A. Angus, J.F. Ni, S.P. Grand, Constraints on the interpretation of S-to-P receiver functions, Geophys. J. Int. (2006), doi:10.1111/j.1365–246X.2006.02981.x.

[19] B.L.N. Kennett, E.R. Engdahl, Travel times for global earthquake location and phase identification, Geophys. J. Int. 105 (1991) 429.

[20] V. Cerveny, Seismic Ray Theory, Cambridge University Press, 2001, pp. 373–375, (relation 4.11.6).

[21] D.E. James, R.W. Carlson, F.B. Boyd, P.E. Janney, Petrologic constraints on seismic velocity variations in the upper mantle beneath Southern Africa? EOS, Trans. — Am. Geophys. Union 82 (2001) S247 (20(Abstract Suppl.)).

[22] R.J. Durrheim, R.W. Green, A seismic refraction investigation of the Archean Kaapvaal Craton, South Africa, using mine tremors as the energy source, Geophys. J. Int. 108 (1992) 812–832.

[23] R.G. Cawthorn, S.J. Webb, Connectivity between the Western and Eastern limbs of the Bushveld Complex, Tectonophysics 330 (2001) 195–209.

[24] T.K. Nguuri, J. Gore, D.E. James, S.J. Webb, C. Wright, T.G. Zengeni, O. Gwavava, J.A. Snoke, Kaapvaal Seismic Group, Crustal structure beneath Southern Africa and its implications for the formation and evolution of the Kaapvaal and Zimbabwe cratons, Geophys. Res. Lett. 28 (N° 13) (2001) 2501–2504.

[25] S.K. Nair, S.S. Gao, K.H. Liu, P.G. Silver, Southern Africa crustal evolution and composition. Constraints from receiver function studies, J. Geophys. Res. 111 (2006) BO2304, doi:10.1029/2005JB003802.

[26] F. Niu, D.E. James, Fine structure of the lowermost crust beneath the Kaapvaal craton and its implications for crustal formation and evolution, Earth Planet. Sci. Lett. 200 (2002) 121–130.

[27] L. Vinnik, V. Farra, Subcratonic low-velocity layer and flood basalts, Geophys. Res. Lett. 29–4 (1049) (2002), doi:10.1029/2001GL014064.

[28] F.R. Boyd, J.J. Gurney, S.H. Richardson, Evidence for a 150–200 km thick Archean lithosphere from diamond inclusion thermobarometry, Nature 315 (1985) 387–389.

[29] D.E. James, F.B. Boyd, D. Schutt, D.R. Bell, R.W. Carlson, Xenolith constraints on seismic velocities in the upper mantle beneath Southern Africa, Geochem. Geophys. Geosyst. 5 (Q01002) (2004), doi:10.1029/2003GC000551.

[30] N.S.C. Simon, G.J. Irvine, G.R. Davies, D.G. Pearson, R.W. Carlson, The origin of garnet and clinopyroxe in "depleted" Kaapvaal peridotites, Lithos 71 (2003) 289–322.

[31] M. Bruneton, H.A. Pedersen, P. Vacher, I.T. Kukkonen, N.T. Arndt, S. Funke, W. Friederich, V. Farra, Svekalapko, Seismic tomography working Group, Layered lithospheric mantle in the central Baltic Shield from surface wave and Xenolith analysis, Earth Planet. Sci. Lett. 226 (2004) 41–52.

[32] P.G. Silver, S.S. Gao, K.L. Liu, Mantle deformation beneath Southern Africa, Geophys. Res. Lett. 28 (13) (2001) 2493–2496.

[33] J. Revenaugh, S. Sipkin, Seismic evidence for silicate melt atop the 410 km mantle discontinuity, Nature 369 (1994) 474–476.

[34] D. Bercovici, S.I. Karato, Whole-mantle convection and the transition-zone water filter, Nature 425 (2003) 39–44.

[35] T. Kawamoto, R. Hervig, J. Holloway, Experimental evidence for a hydrous transition zone in the early earth's mantle, Eart Planet. Sci. Lett. 142 (1996) 587–592.

[36] J. Ritsema, H.J. van Heijst, J.H. Woodhouse, Global transition zone tomography, J. Geophys. Res. 109 (2004) B02302, doi:10.1029/2003JB002610.

[37] S.P. Grand, Mantle shear-wave tomography and the fate of subducted slabs, Phil. Trans. R. Soc. Lond. A 360 (2002) 2475–2491.

[38] R. Rudnick, W. Mc Donough, R. O'Connell, Thermal structure, thickness and composition of continental lithosphere, Chem. Geol. 145 (1998) 395–411.

[39] C. Jaupart, J.C. Mareschal, L. Guillou-Frottier, Heat flow and thickness of the lithosphere in the Canadian shield, J. Geophys. Res. 103 (1998) 15269–15286.

[40] G.L. Kosarev, L.I. Makeyeva, E.F. Savarensky, E.M. Chesnokov, Influence of anisotropy beneath seismograph stations on body waves, (in Russian), Izv. Acad. Nauk, Fizika Zemli 2 (1979) 26–37.